SPECTRUM OF OPTICALLY THIN ADVECTION-DOMINATED ACCRETION FLOW AROUND A BLACK HOLE: APPLICATION TO SAGITTARIUS A*

T. Manmoto and S. Mineshige
Department of Astronomy, Faculty of Science, Kyoto University, Sakyo-ku, Kyoto 606-01, Japan

and

M. Kusunose
Department of Physics, School of Science Kwansei Gakuin Univeristy, 1-155 Uegahara Ichibancho Nishinomiya 662, Japan

Received 4 April 1997; accepted 6 June 1997

ABSTRACT

The global structure of optically thin advection dominated accretion flows which are composed of two-temperature plasma around black holes is calculated. We adopt the full set of basic equations including the advective energy transport in the energy equation for the electrons. The spectra emitted by the optically thin accretion flows are also investigated. The radiation mechanisms which are taken into accout are bremsstrahlung, synchrotron emission, and Comptonization. The calculation of the spectra and that of the structure of the accretion flows are made to be completely consistent by calculating the radiative cooling rate at each radius. As a result of the advection domination for the ions, the heat transport from the ions to the electrons becomes practically zero and the radiative cooling balances with the advective *heating* in the energy equation of the electrons. Following up on the successful work of Narayan et al. (1995), we applied our model to the spectrum of Sgr A*. We find that the spectrum of Sgr A* is explained by the optically thin advection dominated accretion flow around a black hole of the mass $M_{\rm BH} = 10^6 M_\odot$. The parameter dependence of the spectrum and the structure of the accretion flows is also discussed.

Subject headings: accretion, accretion disks — black hole physics — radiation mechanisms: non-thermal — Galaxy: center

1. Introduction

Ever since the pioneering studies of steady thin accretion disks by Shakura & Sunyaev (1973, hereafter SS), the model of thin accretion disks has been applied successfully to low energy emission from astrophysical objects, such as dwarf novie and pre-main-sequence stars. However, the model has been less successful in modeling of high energy emission from Galactic black hole candidates and active galactic nuclei which are considered to be powered by accreting black holes. The main problem lies in the fact that the thin accretion disks can not reproduce the observed spectra of such systems. The thin accretion disk model which SS originally proposed assumes that the disk is optically thick in the vertical direction and radiates the energy generated by the viscosity locally. This model predicts that the generated spectrum is multi-colored black body, which cannot explain the observed power-law spectra of X-rays from AGNs and Galactic black hole candidates even though it can explain the UV bump of the AGN or the soft state spectrum of the Galactic black hole candidates. More fundamentally, although it is generally believed that QSOs and Seyfert galaxies are powered by the gas accretion onto a super-massive black hole of the mass $M_{\rm BH} \sim 10^8 M_\odot$, the thin accretion disks onto such super-massive black holes are too cool to generate high energy photons which are observed in many QSOs and Sayfert galaxies.

The model which is investigated by Shapiro, Lightman & Eardley (1976, hereafter SLE) is quite attractive in that the accreted gas is optically thin and is much hotter than that in the SS solution and is hot enough to produce high energy photons. SLE considered two-temperature plasma with ions being much hotter than electrons, which enabled quantitative studies of the non-blackbody spectra. SLE model has been applied to explain the spectrum of X-ray binaries and active galactic nuclei successfully. However, it is known that the optically thin hot accretion disk which is considered in SLE is thermally unstable (Piran 1978). If the accretion disk is heated up, then the disk expands and the density decreases, so that the bremsstrahlung cooling rate decreases. The reduced cooling then causes the gas to become even hotter, leading to a runaway thermal instability. For this reason it is not likely that such hot accretion disks exist in real systems for much longer than the thermal timescale.

The models introduced so far are local solutions in the sense that the heat generated via viscosity is locally radiated away efficiently, which corresponds to neglecting the advective energy transport in the energy equations. When plasma cannot emit radiation efficiently, the heat generated via viscosity is advected inwards as the internal energy of the plasma. Abramowicz et al. (1988) investigated the effect of advection term in their “slim disk” model in the optically thick case, and made it clear that there exists advection dominated branch where the viscous heating is balanced with the advection term rather than the radiative cooling term at high mass accretion rates.

The optically thin advection dominated solution at low mass accretion rates is studied intensively by Abramowicz et al. (1995) and Narayan &Yi (1995) (see also Ichimaru 1977, Matsumoto et al. 1985). Although they claimed that optically thin advection dominated

solution is thermally stable for the long wavelength perturbations, Kato et al. (1996) showed the possibilities of the instability against the short wavelength perturbations. Manmoto et al. (1996) demonstrated that such an instability is favored for explaining rapid X-ray fluctuations from Galactic black hole candidates and does not affect the global stability of the accretion flows.

The optically thin advection dominated accretion flows are applied to explain the observed spectra of accreting black holes. Narayan & Yi (1995) investigated the self-similar solution which is used later to calculate the spectrum from several low-luminosity accreting systems with great success. As a next step, the calculations of full global steady solutions were awaited for further investigations. Chen et al. (1997) solved optically thin advection dominated solution globally, but their solutions are those of one-temperature plasma and do not include detailed radiation mechanisms. Narayan et al. (1997) derived global solution for optically thin advection dominated accretion flows and showed that the self-similar solution is a good approximation at the radius far enough from the outer and the inner boundaries. This means that the spectra which are derived by using the self-similar solution may be modified, because considerable amount of photons may come from the hot region near the inner boundary. Narayan et al. (1997) did calculate the spectra from two-temperature accretion flows with their global solutions, but they treated the electron energy equations locally, neglecting the effect of the electron advection. Nakamura et al. (1996) were the first to solve the energy equations for ions and electrons and obtained the global two-temperature advection dominated solutions, and showed that the temperature profiles which are crucial to the generated spectra are largely modified when the effect of electron advection is taken into account. However, Nakamura et al. (1996) focused their attentions on the structure of the optically thin accretion disks and did not investigate the spectra from the disks.

The study on the spectrum from optically thin advection dominated accretion flows with full global treatment of the basic equations is yet to be done. Thus we are motivated to consistently solve full set of equations including the energy equation for ions and electrons with detailed radiation mechanisms and obtain the spectra from the optically thin accretion flows.

In section 2, we present the physical assumptions and the basic equations of our model. We show the results of our calculations in section 3. We then apply our model to Sgr A* (the central core of our Galaxy) in section 4. We conclude in section 5 with a summary and discussion.

2. Accretion Flow Model

2.1. Physical Assumptions

We consider an optically thin, steady axisymmetric accretion flow around a black hole. To investigate the spectra generated by the optically thin gas flows, we discuss gas dynamics in the context of two-temperature plasma. Assuming the existence of randomly oriented magnetic fields which possibly originate from the turbulence in the gas flow, we take total pressure p to be

$$p = p_{\rm gas} + p_{\rm mag}, \tag{1}$$

where $p_{\rm gas}$ is the gas pressure, $p_{\rm mag}$ is the magnetic pressure. We neglect the radiation pressure in this paper because the optically thin accretion flows we consider is always gas pressure dominated. We take the ratio of gas pressure to the total pressure as a global parameter which we designate as β. Technically we need to solve the magnetic field self-consistently with the gas dynamics, but it is beyond the scope of this paper to treat full magneto-hydrodynamics equations. Due to the two-temperature assumption, we write $p_{\rm gas}$ as

$$p_{\rm gas} = \beta p = p_i + p_e = \frac{\rho}{\mu_i}\frac{k}{m_{\rm H}}T_i + \frac{\rho}{\mu_e}\frac{k}{m_{\rm H}}T_e. \tag{2}$$

Here and hereafter subscripts i and e indicate the quantities for ions and electrons, respectively. In eq. (2), T is the temperature, ρ is the density, and μ is the mean molecular weight which is given by

$$\mu_i = 1.23, \quad \mu_e = 1.14, \tag{3}$$

where numerical values correspond to the cosmic abundance. We estimate magnetic field B via magnetic pressure by the following equation:

$$p_{\rm mag} = (1-\beta)\,p = \frac{B^2}{8\pi}. \tag{4}$$

2.2. Basic Equations

We adopt cylindrical coordinate system (r,φ,z) to describe axisymmetric ($\frac{\partial}{\partial\varphi} = 0$) accretion flows. Basic equations which describe the dynamics of the accretion disks are those of mass conservation, Euler equations which comprises three spatial components, and the energy equations. Mass conservation gives

$$\frac{\partial}{\partial r}\left(r\rho v_r\right) + r\frac{\partial}{\partial z}\left(\rho v_z\right) = 0, \tag{5}$$

where v_r and v_z are the radial and the vertical velocity respectively. The radial component of Euler equation is

$$\frac{\partial}{\partial r}\left(r\rho v_r^2\right) + r\frac{\partial}{\partial z}\left(\rho v_r v_z\right) = -\rho\left(r\frac{\partial\psi}{\partial r} - v_\varphi^2\right) - r\frac{\partial p}{\partial r}, \tag{6}$$

where v_φ is the azimuthal velocity and ψ is the potential energy. To simulate general relativistic effects, we adopt pseudo-Newtonian potential

$$\psi = -GM_{\rm BH}/(R - r_{\rm g}) \tag{7}$$

with $M_{\rm BH}$ being the mass of the black hole, $r_{\rm g}$ the Schwarzschild radius, and $R = (r^2 + z^2)^{1/2}$ the distance from the central black hole. This potential is known to represent the dynamical aspects of general relativistic effects quite well for $r > 2r_{\rm g}$ (Paczyński & Wiita 1980) and greatly simplifies the basic equations. Technically we need to solve the basic equations in the Schwarzschild or Kerr metric especially for the photon propagation. However solving the equations including the photon propagation in the full relativisitc metric is out of the scope of current paper. Azimuthal component of Euler equation is the conservation of angular momentum which gives

$$\frac{\partial}{\partial r}\left(r^2 \rho v_r v_\varphi\right) + r\frac{\partial}{\partial z}\left(r\rho v_\varphi v_z\right) = \frac{\partial}{\partial r}\left(r^2 \tau_{r\varphi}\right). \tag{8}$$

Here $\tau_{r\varphi}$ is the $r\varphi$-component of the stress tensor. According to the conventional *alpha*-prescription of sheer viscosity, $\tau_{r\varphi}$ can be written as

$$\tau_{r\varphi} = \alpha p \frac{d\ln\Omega}{d\ln r}\frac{\Omega}{\Omega_k}, \tag{9}$$

where Ω is the angular velocity and $\Omega_{\rm K}$ is the Keplerian angular velocity on the equatorial plane. In our paper, we take $\tau_{r\varphi}$ to be simply proportional to the local pressure p:

$$\tau_{r\varphi} = -\alpha p, \tag{10}$$

where α is the dimensionless viscosity parameter which in general is considered to be around $0.01 \sim 0.1$. Two-temperature assumption requires two energy equations i.e. one for ions and one for electrons, both of which contain advective energy transport terms. The energy equation for each species is

$$\rho T_i\left(v_r\frac{\partial s_i}{\partial r} + v_z\frac{\partial s_i}{\partial z}\right) = \tau_{r\varphi} r\frac{\partial\Omega}{\partial r} - \lambda_{ie}, \tag{11}$$

$$\rho T_e\left(v_r\frac{\partial s_e}{\partial r} + v_z\frac{\partial s_e}{\partial z}\right) = \lambda_{ie} - q_{\rm rad}^-, \tag{12}$$

where s is the specific entropy, λ_{ie} is the volume energy transfer rate from ions to electrons, and $q_{\rm rad}^-$ is the volume radiative cooling rate. We assume that the energy is transferred from ions to electrons via Coulomb collisions only. Stepney & Guilbert (1983) give an explicit expression:

$$\begin{aligned}\lambda_{ie} &= 1.25 \times \tfrac{3}{2}\tfrac{m_e}{m_p} n_e n_i \sigma_{\rm T} c \tfrac{(kT_i - kT_e)}{K_2(1/\theta_e)K_2(1/\theta_i)} \ln\Lambda \\ &\times \left[\tfrac{2(\theta_e+\theta_i)^2+1}{(\theta_e+\theta_i)} K_1\left(\tfrac{\theta_e+\theta_i}{\theta_e\theta_i}\right) + 2K_0\left(\tfrac{\theta_e+\theta_i}{\theta_e\theta_i}\right)\right]\end{aligned} \tag{13}$$

where the K's are modified Bessel functions, $\ln \Lambda = 20$ is the Coulomb logarithm, and $\theta \equiv kT/m_e c^2$ is the dimensionless temperature. Note that the energy equations assume that the ions and the electrons are in thermal equilibrium by some mechanisms. The thermodynamic relations are

$$\rho T_i ds_i = \frac{1}{\gamma - 1}\left(dp_i - \gamma \frac{p_i}{\rho} d\rho\right), \tag{14}$$

$$\rho T_e ds_e = \frac{1}{\gamma - 1}\left(dp_e - \gamma \frac{p_e}{\rho} d\rho\right), \tag{15}$$

where $\gamma = 5/3$ is the adiabatic index. In the energy equations we have assumed viscous heating acts only on ions because an ion particle is much heavier than an electron particle.

Now we have full set of basic equations which describe the steady accretion flow around a black hole. However, it is rather a difficult problem to solve above partial differential equations with respect to r and z plus radiative transfer equations to obtain global steady solutions. To lessen the number of variables, we fix the vertical structure before we solve the full spatial equations, assuming the accretion flow is geometrically thin. The validity of the assumption that the disk is geometrically thin will be discussed later. As a first order approximation, we adopt isothermal structure in the vertical direction, which means that the sound velocity $c_{\rm s} \equiv (p/\rho)^{1/2}$ is independent of z. Furthermore, we also assume radial and azimuthal velocities are independent of z. The vertical structure is obtained analytically by solving the remaining vertical component of Euler equation which represents hydrostatic balance in the vertical direction:

$$\frac{\partial p}{\partial z} = -\rho \frac{\partial \psi}{\partial z} = -\rho {\Omega_{\rm K}}^2 z. \tag{16}$$

The last equation of eq. (16) assumes that the disk is geometrically thin. The density distribution in the vertical direction is

$$\rho\left(r, z\right) = \rho\left(r, 0\right) \exp\left(-\frac{z^2}{2H^2}\right). \tag{17}$$

Here, H is the vertical scale height defined by

$$H \equiv c_s/\Omega_{\rm K}. \tag{18}$$

With the vertical structure given above, we can now integrate above basic equations in the vertical direction and rewrite them as follows. Mass conservation now gives

$$\dot{M} = 2\pi r \Sigma v_r, \tag{19}$$

where $\Sigma\left(r\right) \equiv \int_{-\infty}^{\infty} \rho\left(r, z\right) dz = 2\sqrt{\pi/2}\rho\left(r, 0\right) H$ is the surface density. We have taken v_r to be positive for the inward flow so that the mass accretion rate $\dot{M}$ takes positive value. The height-integrated version of the radial component of eq. (6) is

$$v_r \frac{dv_r}{dr} + \frac{1}{\Sigma}\frac{dW}{dr} = r\left(\Omega^2 - {\Omega_{\rm K}}^2\right) - \frac{W}{\Sigma}\frac{d \ln \Omega_{\rm K}}{dr}, \tag{20}$$

where $W(r) \equiv \int_{-\infty}^{\infty} p(r,z)dz = 2\sqrt{\pi/2}p(r,0)\,H$ is the height-integrated pressure. The last term of the right hand side of eq. (20) corresponds to the correction for the decrease of the radial component of gravitational force away from the equatorial plane (Matsumoto et al. 1984). We can integrate the conservation of angular momentum (eq. [8]) with respect to r as well as z and obtain following simple equation:

$$\dot{M}\left(l - l_{\rm in}\right) = 2\pi r^2 \alpha W, \tag{21}$$

where $l_{\rm in}$ is the specific angular momentum swallowed by the central black hole. The energy equations (eq. [11], [12]) are vertically integrated together with the thermodynamic relations (eq. [14], [15]) and now can be written as

$$\dot{M}\frac{W_i}{\Sigma}\left(\frac{\gamma+1}{2(\gamma-1)}\frac{d\ln W_i}{dr} - \frac{3\gamma-1}{2(\gamma-1)}\frac{d\ln\Sigma}{dr} - \frac{d\ln\Omega_k}{dr}\right) = \dot{M}\left(l-l_{\rm in}\right)\frac{d\Omega}{dr} + 2\pi r\Lambda_{ie}, \tag{22}$$

$$\dot{M}\frac{W_e}{\Sigma}\left(\frac{\gamma+1}{2(\gamma-1)}\frac{d\ln W_e}{dr} - \frac{3\gamma-1}{2(\gamma-1)}\frac{d\ln\Sigma}{dr} - \frac{d\ln\Omega_k}{dr}\right) = 2\pi r\left(Q^-_{\rm rad} - \Lambda_{ie}\right), \tag{23}$$

where $\Lambda_{ie} \equiv \int_{-\infty}^{\infty} \lambda_{ie}(z)dz = \sqrt{\pi}H\lambda_{ie}(0)$ is the energy transfer rate from ions to electrons per unit surface area. $Q^-_{\rm rad}$ is the radiative cooling rate per unit surface area which will be explicitly given in the next subsection. The energy equations can be written compactly as follows:

$$Q^-_{{\rm adv},i} = Q^+_{\rm vis} - \Lambda_{ie}, \tag{24}$$

$$Q^-_{{\rm adv},e} = \Lambda_{ie} - Q^-_{\rm rad}. \tag{25}$$

2.3. Radiation Mechanism

Following the work of Narayan & Yi (1995), we consider three processes for radiative cooling: bremsstrahlung, synchrotron radiation, and Comptonization of soft photons. In order to obtain the spectrum generated by the accretion flow and the global structure of the accretion disk, we need to solve global radiation transfer problem in the radial and the vertical direction which involves self-absorption and incoherent scatterings. We treat such complicated problem in a rather simplified way: 1) we assume locally plane parallel gas configuration at each radius and 2) we separate the Compton scattering process from the rest of radiation processes, i.e. emission and absorption. This will not make serious error because the gas is so tenuous that generated photons rarely experience multiple scatterings before they escape. Note that at such low frequencies as radio frequencies, the effect of free-free and synchrotron self-absorption is so large that the disk can not be considered optically thin, while the optical depth for scatterings is constant at all frequencies. We first estimate the spectrum of unscattered photons at given radius by solving radiative diffusion equation in the vertical direction. For the isothermal plane parallel gas atmosphere where

density configuration is given by eq. (17) the radiative diffusion equation can be solved and gives the energy flux F_ν of the unscattered photons at given radius (see Appendix B):

$$F_\nu = \frac{2\pi}{\sqrt{3}} B_\nu \left[1 - \exp\left(-2\sqrt{3}\tau_\nu^*\right)\right], \tag{26}$$

where $\tau_\nu^* \equiv \frac{\sqrt{\pi}}{2}\kappa_\nu(0)H$ is the optical depth for absorption of the accretion flow in the vertical direction with $\kappa_\nu(0)$ being the absorption coefficient on the equatorial plane. Assuming LTE, we can write $\kappa_\nu = \chi_\nu / (4\pi B_\nu)$ where $\chi_\nu = \chi_{\nu,\mathrm{brems}} + \chi_{\nu,\mathrm{synch}}$ is the emissivity. Note that equation (26) includes the effects of free-free absorption and synchrotron self-absorption at low frequencies.

2.3.1. Bremsstrahlung Emission

In our model, electron temperature exceeds rest mass energy of an electron in some cases where electron-electron bremsstrahlung is important as well as electron-proton bremsstrahlung which dominates electron-electron bremsstrahlung in the classical temperature regime. Thus the cooling rate per unit volume for bremsstrahlung is

$$q_{\mathrm{br}}^- = q_{ei}^- + q_{ee}^-. \tag{27}$$

Following Narayan & Yi (1995), we employ

$$q_{ei}^- = 1.25 n_e^2 \sigma_{\mathrm{T}} c \alpha_f m_e c^2 F_{ei}(\theta_e), \tag{28}$$

where α_f is the fine-structure constant and F_{ei} is given by

$$F_{ei}(\theta_e) = 4\left(\frac{2\theta_e}{\pi^3}\right)^{1/2}\left(1 + 1.781\theta_e^{1.34}\right) \quad for\ \theta_e < 1, \tag{29}$$

$$F_{ei}(\theta_e) = \frac{9\theta_e}{2\pi}\left[\ln(1.123\theta_e + 0.48) + 1.5\right] \quad for\ \theta_e > 1, \tag{30}$$

and

$$\begin{aligned} q_{ee}^- &= n_e^2 c r_e^2 \alpha_f c^2 \tfrac{20}{9\pi^{1/2}} \left(44 - 3\pi^2\right)\theta_e^{3/2} \\ &\times \left(1 + 1.1\theta_e + \theta_e^2 - 1.25\theta_e^{5/2}\right) \quad for\ \theta_e < 1, \end{aligned} \tag{31}$$

$$q_{ee}^- = n_e^2 c r_e^2 \alpha_f c^2 24\theta_e \left(\ln 1.1232\theta_e + 1.28\right) \quad for\ \theta_e > 1. \tag{32}$$

With the cooling rate given above, we can write the emissivity $\chi_{\nu,\mathrm{brems}}$ as

$$\chi_{\nu,\mathrm{brems}} = q_{\mathrm{br}}^- \bar{G} \exp\left(\frac{h\nu}{kT_e}\right), \tag{33}$$

where $\bar{G}$ is the Gaunt factor which is given by (see Rybicki & Lightman 1979)

$$\bar{G} = \frac{h}{kT_e}\left(\frac{3}{\pi}\frac{kT_e}{h\nu}\right)^{1/2} \qquad for\ \frac{kT_e}{h\nu} < 1, \tag{34}$$

$$\bar{G} = \frac{h}{kT_e}\frac{\sqrt{3}}{\pi}\ln\left(\frac{4}{\zeta}\frac{kT_e}{h\nu}\right) \qquad for\ \frac{kT_e}{h\nu} > 1. \tag{35}$$

2.3.2. *Synchrotron Emission*

For the relativistic temperatures for the electrons, and in the presence of magnetic field which is of the same order as equipartition magnetic field, synchrotron emission is also very important. Following Narayan & Yi (1995), the optically thin synchrotron emissivity by a relativistic Maxwellian distribution of electrons is

$$\chi_{\nu,\mathrm{synch}} = 4.43 \times 10^{-30}\frac{4\pi n_e \nu}{K_2\left(1/\theta_e\right)} I'\left(\frac{4\pi m_e c\nu}{3eB\theta_e^2}\right), \tag{36}$$

where $I'(x)$ is given by

$$I'\left(x\right) = \frac{4.0505}{x^{1/6}}\left(1 + \frac{0.4}{x^{1/4}} + \frac{0.5316}{x^{1/2}}\right)\exp\left(-1.8899x^{1/3}\right). \tag{37}$$

2.3.3. *Compton Scattering*

We proceed to consider the effect of Compton scattering. We make use of the idea of energy enhancement factor which is derived by Dermer, Liang, & Canfield (1991) and modified in part by Esin et al. (1996). The energy enhancement factor η is defined as the average energy boost of a photon. The prescription for η is

$$\eta = \exp\left(s\left(A-1\right)\right)\left[1 - P\left(j_\mathrm{m}+1, As\right)\right] + \eta_\mathrm{max}P\left(j_\mathrm{m}+1, s\right), \tag{38}$$

where P is the incomplete gamma function and

$$\begin{aligned} A &= 1 + 4\theta_e + 16\theta_e^2, \\ s &= \tau_\mathrm{es} + \tau_\mathrm{es}^2, \\ \eta_\mathrm{max} &= \tfrac{3kT_e}{h\nu}, \\ j_\mathrm{m} &= \tfrac{\ln(\eta_\mathrm{max})}{\ln(A)}. \end{aligned} \tag{39}$$

τ_{es} is the optical depth for scattering:

$$\tau_{\rm es} = 2n_e\sigma_{\rm T}H \times \max\left(1, \frac{1}{\tau_{\rm eff}}\right), \tag{40}$$

where $\tau_{\rm eff} \equiv \tau_\nu \left(1 + n_e\sigma_{\rm T}/\kappa_\nu\right)^{1/2}$ is the effective optical depth (Rybicki & Lightman 1979). Equation (37) gives the correct estimate for the optical depth for scattering in the presence of the absorption. Note that the simple treatment given above assumes that the cross-section is Thomson cross-section rather than exact Klein-Nishina cross-section. With the energy enhancement factor η, the local radiative cooling rate $Q^-_{\rm rad}$ is given by

$$Q^-_{\rm rad} = \int d\nu\eta\left(\nu\right)2F_\nu. \tag{41}$$

We calculate the radiative cooling rate numerically and use it for the energy equation for electrons at each radius to calculate the global solution of the accretion flows.

2.3.4. Calculation of the Spectrum

We need more detailed specification for the calculation of the spectrum. Knowing the spectrum of unscattered photons and the probability that a photon will suffer scattering given times, we can calculate the Compton scattered spectrum if we know the information about how the original spectrum is modified after experiencing one scattering. Note that the average energy boost given in (36) is the energy boost *averaged* over the Maxwellian distribution of electrons and can not be used directly for the spectrum calculations. Such problem was precisely discussed first by Jones (1968) and corrected afterwards by Coppi & Blandford (1990). We make use of the formula given by Coppi & Blandford (1990) and calculate the resulting spectrum. The remaining problem concerning Compton scattering is how to treat the spectrum of the saturated Comptonized photons. We assume that photons which are scattered more than j_m times saturate and obey the Wien distribution $\propto \nu^3 \exp\left(-h\nu/kT_e\right)$.

Since large fraction of the emitted radiation is generated at the radius fairly close to the black holes in our model, we cannot ignore the effect of redshift due to the gravity and the gas motion. We include the gravitational redshift by simply taking the ratio of the energy of a photon when observed to its energy emitted at radius r to be $\sqrt{1 - r_{\rm g}/r}$. To treat redshift due to relativistic gas motion in a simple way, we concentrate on the face-on case where the optically thin assumption is most adequate. Thus we simply take the ratio of energy change for the redshift due to gas motion to be $1/\sqrt{1-(v/c)^2}$.

2.4. Numerical Procedure

We solve numerically the set of equations given so far with the boundary conditions. The outer boundary conditions imposed are

$$\Omega = 0.8\Omega_{\rm K}, \tag{42}$$

$$T_{\rm gas} \equiv \mu \left(\frac{T_i}{\mu_i} + \frac{T_e}{\mu_e} \right) = 0.1 T_{\rm vir}, \tag{43}$$

$$Q^-_{\rm rad} = \Lambda_{ie} \tag{44}$$

at $r_{\rm out} = 10000 r_{\rm g}$. Here $T_{\rm vir}$ is the virial temperature defined by

$$T_{\rm vir} \equiv (\gamma - 1) \frac{G M_{\rm BH} m_{\rm H}}{kr} \tag{45}$$

We did not set the angular velocity to be the Keplerian angular velocity itself at the outer boundary for simply technical reasons. We need to set somewhat sub-Keplerian disk at the outer boundary so that the viscous heating term take positive value with the simple viscosity prescription adopted in this paper [eq. (10)]. We confirmed that the outer boundary condition have little effect on the structure of the inner advection-dominated flows. There have been many suggestions about how outer Keplerian disks are connected to the advection dominated disks. For instance, Honma (1996) took into account the effect of thermal conductivity and obtained the global solutions where the outer cool Keplerian disk is connected to the inner hot optically thin disk. However the mechanism of the transition is not yet clear.

The free parameters in the set of equations are α, β, $M_{\rm BH}$, $\dot{M}$, and $l_{\rm in}$. These five parameters are not independent because of the transonic nature of the equations. $l_{\rm in}$ can be determined uniquely so that the solution should satisfy the transonic condition when the remaining parameters are given. We have to adjust $l_{\rm in}$ recursively to obtain smooth transonic solutions, since the location of the transonic point is not known until we obtain global transonic solutions.

3. Results

To discuss the general properties of our model, we set $m \equiv M_{\rm BH}/M_\odot = 10^8$ and $\dot{m} \equiv \dot{M}/\dot{M}_{\rm c} = 10^{-4}$ where $\dot{M}_{\rm c} \equiv 32\pi c r_{\rm g}/\kappa_{\rm es}$ and assign typical values for other parameters: $\alpha = 0.1$, $\beta = 0.5$ (case of equipartition). To demonstrate how the heatings and coolings balance in the energy equations, we show Figure 1 the Q's for the ions (upper panel), and for the electrons (lower panel); (see eq. [25]). The solid line in the upper panel shows the ratio of advective cooling of ions to the viscous heating, which is commonly denoted by f.

We have $f = 1$ for the purely advection dominated accretion flows and $f = 0$ for the purely radiative cooling dominated accretion flows. We see that f asymptotically approaches unity as the radius decreases. We use the region $r < 2000 r_{\rm g}$ to investigate the spectrum from the optically thin advection dominated accretion flows. We see from Figure 1 that the accretion flows becomes highly advection dominated in the region $r < 100 r_{\rm g}$ where the heat transport from ions to electrons by the Coulomb coupling practically becomes zero. The interesting point is that it is electron advective *heating*, rather than the heat supplied from the ions, that balances with the radiative cooling of electrons, which means the electron accretion flow becomes cooling flow near the central black hole where the electrons are cooled by consuming the stored internal energy to radiate before being heated up by the ions (cf. Nakamura et al. 1997). Many analyses concerning two-temperature accretion flows have adopted simplified energy equation for electrons: $\Lambda_{ie} = Q^-_{\rm rad}$. Our results shows that above simplified energy equation is inadequate for the analysis of two-temperature advection dominated flows and one should adopt $Q^-_{{\rm adv},e} = -Q^-_{\rm rad}$ instead.

Figure 2 shows the ion and electron temperature profiles. We see that the electron temperature is heated up to $T_e \sim 10^{10}$K. Although we need to include the effect of electron-positron pair production and annihilation for such hot accretion flows, we make simple assumption that the pair density is very low (see discussion in Esin et al. 1996, Bjornsson et al. 1996, Kusunose & Mineshige 1996).

Figure 3 shows the aspect ratio h/r of the accretion flow. We have used height-integrated equations for our calculations which neglect the higher order of h/r. We may conclude that the value of h/r shown in Figure 3 is marginally safe for the height integration. However, of course, the vertical structure of the advection dominated accretion flows is an important issue and we will investigate it in future papers.

Figure 4 shows the angular momentum and the various velocities as a function of the radius r. Here $c_{\rm s}^*$ is defined as

$$c_{\rm s}^* \equiv \left(\frac{(3\gamma - 1) + 2\,(\gamma - 1)\,\alpha^2}{\gamma + 1} \frac{W}{\Sigma} \right)^{1/2}, \tag{46}$$

so that $v_r = c_{\rm s}^*$ at the critical point. We see from the Figure 4 that the radial dependence of the radial and the azimuthal velocities are different from that of the self-similar solutions, in which all the velocities are proportional to $r^{-1/2}$, especially in the super-sonic region. We see that for the parameters given above, the azimuthal velocity v_φ is fairly sub-Keplerian and even sub-sonic and of the same order as the radial velocity v_r unlike the standard model, which is known to be a common feature for $\alpha = 0.1$. (In the standard model, we have $v_\varphi \sim r\Omega_{\rm K} = c_{\rm s}^* h/r \gg c_{\rm s}^* \gg v_r$.) Note that we have 'sub-sonic' azimuthal velocity when the rotation is highly sub-Keplerian ($v_\varphi < r\Omega_{\rm K}$) and the disk is hot and geometrically thick ($h/r \sim 1$). For the reason that the radial velocity v_r is the same order as the azimuthal velocity v_φ, we call the accreting gas "accretion flow" rather than to call "accretion disk" in this paper.

Figure 5 illustrates the luminosity distribution as a function of r. The contributions from respective radiation mechanisms (i.e. bremsstrahlung, synchrotron, Comptonization) are also shown. We see that the bremsstrahlung emission is important and the effect of the synchrtron emmision and the Comptonization is negligibly small in the outer region of the accretion flow ($r > 10r_{\rm g}$), while the synchrotron emission and the Comptonization dominate in the hot inner region ($r < 10r_{\rm g}$). The contribution of the Comptonization rapidly increases as the radius decreases because the amount of the synchrotron soft photons increases and not because the Compton y-parameter $y \equiv \tau_{\rm es} kT_e/m_e c^2$ increases. Note that in the innermost region the electron temperature T_e is approximately constant and the surface density decreases and thereby y actually decreases. Note that almost all emission comes from the hot inner region ($r < 10r_{\rm g}$) and the fraction of the emission from the super-sonic region, which the self-similar solutions fail to describe accurately, is fairly large. As far as the bremsstrahlung is concerned, the contribution of the emission from the large radii is not negligible, which make the slope of the bremsstrahlung spectrum less steep, since what we observe is the superposition of the bremsstrahlung peaks from different radii.

In Figure 6, we shows the spectrum generated by the optically thin accretion flows. Parameters are $m = 10^8$, $\dot{m} = 10^{-4}$, $\alpha = 0.1$, $\beta = 0.5$. S indicates the synchrotron peak which is composed of Rayleigh-Jeans slope and the optically thin synchrotron emission. C1 and C2 indicate the once and twice Compton scattered photons, respectively. B indicates the bremsstrahlung emission plus photons suffering multiple Compton scattering. W indicates saturated Comptonized photons which form Wien tail.

The upper panel of Figure 7 shows the surface density of the accretion flow. The dashed line corresponds to the case with the central black hole mass of $M_{\rm BH} = 10M_\odot$. We find that the structure of the accretion flow is nearly the same when the radius and the mass accretion rate are scaled with the Schwarzschild radius and the critical mass accretion rate, respectively. However we see in the lower panel of the Figure 7 that the electron temperature at the innermost region is varied slightly. This is due to the fact that the accretion flow is highly advection dominated. We remind the readers that the viscous heating is balanced almost entirely with the advective cooling in the ion energy equation and there is little coupling between the ions and the electrons. Thus the structure of the accretion flow is governed by ion energy equation while the electron energy equation including the radiative cooling is decoupled and determines the electron temperature. Although the height-integrated quantities are the same when the radius is scaled with the Schwarzschild radius, the amount of radiative cooling, which is the function of the density distribution rather than the height-integrated quantities, is different. Thus we have different electron temperatures for different black hole masses. We show the spectrum from the accretion flow for the $10M_\odot$ case in Figure 8. The shape of the spectrum is essentially the same as the $10^8 M_\odot$ case, but the position of the synchrotron peak and the absolute luminosity differs considerably.

4. Application to Sagittarius A*

Following up on the successful work of Narayan et al. (1995) which applied the advection dominated model to the Sgr A* (the central core of our Galaxy), we improve their model by fully solving the basic equations to explain the observed emission from radio frequencies to Gamma-rays. Figure 9 shows the model which explains observed radio and X-ray data quite well. The parameters assigned are given in the figure. The points and the short lines are the observational data, which assume interstellar absorption $N_H = 6 \times 10^{22} cm^{-2}$ and a distance $d = 8.5$kpc, both typical for the Galactic Center, compiled by Narayan et al. (1995) (references therein). The various lines correspond to the different values of mass accretion rate which varies by factor of 2. As Narayan et al. noticed, the position of the Rayleigh-Jeans slope is determined solely by the mass of the central black hole. Thus to give a good fit to the observed radio emission with our model, we have no choice but to fix the mass of the central black hole to be $M_{\rm BH} = 10^6 M_\odot$. Considering the inaccuracy of the potential at the innermost region of the accretion flow, this value is consistent with the value which is derived from the gas and stellar dynamics (Genzel & Townes 1987). We have $\dot{M}_{\rm c} = 3.5 \times 10^{-2} M_\odot$/yr for the black hole of the mass $M_{\rm BH} = 10^6 M_\odot$, hence the predicted mass accretion rate is $\sim 2 - 5 \times 10^{-6} M_\odot$/yr.

Figure 9 also illustrates the $\dot{M}$ dependence of our model. The surface density sensitively depends on $\dot{M}$, while the temperature is fairly insensitive to $\dot{M}$. Thus the luminosity at all frequencies decreases when we reduce the mass accretion rate. We find that if we change the mass accretion rate by a factor of ~ 2, X-ray luminosity varies by the same factor while the synchrotron peak varies little. We suggest that the various X-ray data seemingly inconsistent with each other are purely due to the change of the mass accretion rate of the accretion flow. There have been an argument that the X-ray luminosity of Sgr A* is variable on the timescale of half a year, which is consistent with our suggestion.

Figure 10 illustrates how the spectrum changes with different black hole masses. As we mentioned before, the structure of the accretion flow is the same with proper scalings, but the electron temperature is slightly different because of the difference of the emissivity. We see clearly that the position of the Rayleigh-Jeans slope is determined by the mass of the central black hole.

We show in Figure 11 the β-dependence of the structure of the accretion flow and the spectrum. We remind the readers that the parameter β is defined as the ratio of the gas pressure to the total pressure. We have the stronger magnetic field for the smaller value of β. Unlike the other parameter dependence, the ion temperature as well as the electron temperature decreases when we lower the value of β. This is reasonable because for the lower value of β, the stronger becomes the magnetic pressure and the gas pressure can be smaller to support the accretion flow. This temperature change has a large effect on the bremsstrahlung spectrum but has little effect on the synchrotron peak, which is because the effects of the stronger (weaker) magnetic field and the lower (higher) temperature roughly cancel out. We set $T_{\rm gas} = 0.2 T_{\rm vir}$ at the outer boundary for $\beta = 0.95$ since we could not find

advection dominated solution for $\beta = 0.95$ with $T_{\rm gas} = 0.1T_{\rm vir}$.

Narayan et al. (1995) did not investigate the parameter dependence of the viscosity parameter α and the mass accretion rate $\dot{M}$ independently, since they used simplified disk model, in which α and $\dot{M}$ cannot be chosen independently. Thus it is meaningful to study the α dependence of the spectrum. We show in Figure 12 the α-dependence of our model. When α is large, the angular momentum is extracted efficiently and the surface density decreases, which makes the bremsstrahlung emission weak. However, the increase of the electron temperature at the innermost region makes the synchrotron emission stronger. We find that the width of the synchrotron peak is the most sensitive to the value of α. The upper limits in the radio frequency band imposes strong restriction upon the value of α for the case of Sgr A*. For instance, we can not fit the entire spectrum with $\alpha = 0.1$. We have to set $\alpha < 0.025$ to explain entire spectrum of Sgr A* with our model. This fact is important because it is claimed that $\alpha \sim 0.1$ in advection-dominated accretion flows on various grounds (see discussions in Narayan 1996). If we are to set $\alpha = 0.1$, we have to reduce the mass accretion rate by factor of 4 so as to give a good fit to the observed radio and IR spectrum (see Figure 12). In that case, we cannot explain the X-ray emission from the Galactic Center. Various X-ray observations have found the X-ray sources at the Galactic Center but the angular resolution has been insufficient to identify a source with the radio source Sgr A*. There remains the possibility that X-rays do not come from Sgr A* at all (e.g. see Duschl et al. 1996). If that is the case, all the X-ray data are merely upper limits and the accretion flows with $\alpha = 0.1$ do not conflict with the observations.

There exist some data points in near IR and radio frequencies which cannot be accounted for. However, it is natural to think that there must be dust region or stellar contamination or non-thermal objects like jets in central region of our Galaxy overlapping the accreting black hole which in total we observe as a point source Sgr A*. In that sense, one should consider the observational data as upper limits. A point worth emphasizing here is that the entire spectrum of Sgr A* is basically explained with an optically thin accretion flow around a black hole of the mass $M_{\rm BH} = 10^6 M_\odot$. Moreover, we have solved globally the basic equations including the gas dynamics and the radiation processes consistently rather than to consider more primitive models like isothermal gas complex of certain size.

5. Summary and Discussion

In this paper, we have calculated the global structure of optically thin advection dominated accretion flows in the context of two-temperature plasma, adopting the full set of basic equations including the energy equation for the electrons. We have also calculated the spectra emitted by the optically thin accretion flows which we calculated. We have made the calculation of the spectra and that of the structure of the accretion flows to be completely consistent by calculating the radiative cooling rate at each radius by numerically

integrating the whole spectrum emitted at the radius.

As a result of the advection domination for the ions, the heat transport from the ions to the electrons becomes practically zero and the radiative cooling balances with the advective *heating* of the electrons. This means that the electron cools itself by releasing the stored internal energy as a radiation. Hence the energy equation for the electrons play an important role for the calculation of the spectra, where the temperature profile of the electron is the important factor.

An interesting feature of the advection dominated flow, which is known already, is that the azimuthal velocity becomes highly sub-Keplerian and of the same order as the radial velocity and the sound velocity. The point worth noting is that in the innermost hot luminous region, the divergence of the velocities from those in the self-similar solution is fairly large.

The accreting gas becomes very hot. The electron temperature even exceeds the rest mass energy of an electron. We have not taken into account the effect of the pair production and the annihilation, which is an important issue. For such hot accretion flows, the synchrotron emission and the Compton scattering are very important.

The spectrum is composed by 1) the synchrotron peak which comprises optically thin synchrotron emission and the self-absorbed Rayleigh-Jeans slope and 2) the unsaturated Comptonized photons which forms some bumps and 3) the bremsstrahlung emission and 4)the saturated Comptonized photons. The dependence of the each component on the model parameters is complex. Among them, the position of the Rayleigh-Jeans slope is almost solely determined by the mass of the central black hole. When we make the magnetic field stronger, the temperature of the entire flow decreases, which has significant effect on the Comptonization and the bremsstrahlung emission, but has little effect on the synchrotron emission. When we make the viscosity smaller, the surface density increases and the bremsstrahlung emission increases, but the synchrotron emission and the Comptonization decreases. The simplest relation is the dependence on the mass accretion rate. When we reduce the mass accretion rate, the entire emission is reduced. However the bremsstrahlung emission is much more sensitive to the change of the mass accretion rate than the synchrotron emission.

We find that the spectrum of Sgr A* is explained by the optically thin advection dominated accretion flow around a black hole of the mass $M_{\rm BH} = 10^6 M_\odot$. Narayan et al. (1995) also calculated the spectrum of Sgr A* using an optically thin advection dominated accretion flow model. Their best fit parameters are different from ours. For instance the mass of the central black hole is $M_{\rm BH} = 7.0 \times 10^5 M_\odot$ according to their model. The different points in our model are 1) full global treatment of the basic equations and 2) inclusion of the electron energy equation and 3) calculation of the innermost region where the flow is supersonic and the effects of the redshift are important. 2) and 3) have very important effect on the emitted spectrum, which is not considered in Narayan et al. (1995). We conclude that the X-ray data obtained by various satellite observations are explained by the

variation of the mass accretion rate by a factor of ~ 2, if we allow α to have small value. If we set $\alpha \sim 0.1$, which is considered to be a standard value for the advection dominated accretion flows, it is not likely that the X-rays come from Sgr A*.

We have computed the model using height-integrated equations with fixed structure in the vertical direction. We have also adopted simplified form of equations for the radiation field. Our immediate goal is to solve the basic equations including equations for the radiation field in at least two dimensional space. However, our successful result presented in this paper tells us that the basic idea is correct. The full treatment of Schwarzschild or Kerr metric is also an important issue.

We thank Professor Shoji Kato for useful discussions, and Ann Esin and Jun Fukue for useful comments. We are very grateful to R. Narayan for providing us with a code to calculate inverse-Compton spectra. We thank the referee J. P. Lasota for many valuable comments and suggestions.

A. Height Integrations of the Basic Equations

In this paper, we have adopted the height-integrated equations to obtain the structure of the optically thin advection dominated accretion flows. We have seen that the temperature of the accretion flows is very high and the aspect ratio h/r is ~ 0.5. Thus the height-integration may not be an excellent approximation since the operation of the height-integration omits the higher orders of h/r. Thus we consider it useful to describe in detail the operation of the height-integration to discuss the reliability of our calculations.

The potential we adopted is spherically symmetric, while we adopt the cylindrical coordinate system. Thus we need to expand it around the equatorial plane ($z = 0$) in order to integrate the basic equations in the vertical direction. In the case of geometrically thin accretion flows, we can neglect the terms containing the higher orders of z/r and the operation of the height-integration becomes very simple.

The potential ψ is expanded as

$$\psi\left(r,z\right) = \psi\left(r,0\right)\left[1 + \frac{1}{2}\left.\frac{\partial \ln \psi}{\partial \ln r}\right|_{z=0}\frac{z^2}{r^2} + O\left(\frac{z^4}{r^4}\right)\right]. \tag{A1}$$

Thus we approximate ψ as

$$\psi\left(r,z\right) = \psi\left(r,0\right) + \frac{1}{2}\Omega_k^2 z^2, \tag{A2}$$

where Ω_k is defined as

$$\Omega_k \equiv \left.\left(\frac{1}{r}\frac{\partial \psi}{\partial r}\right)^{1/2}\right|_{z=0}. \tag{A3}$$

Using Equation (A.1), the derivatives of ψ are also expanded as follows:

$$\frac{\partial\psi}{\partial r} = \left.\frac{\partial\psi}{\partial r}\right|_{z=0}\left[1+\frac{d\ln\Omega_k}{d\ln r}\frac{z^2}{r^2}+O\left(\frac{z^4}{r^4}\right)\right], \tag{A4}$$

$$\frac{\partial\psi}{\partial z} = \left.\frac{\partial\psi}{\partial r}\right|_{z=0}\frac{z}{r}\left[1+O\left(\frac{z^3}{r^3}\right)\right]. \tag{A5}$$

We approximate the derivatives of ψ as follows:

$$\frac{\partial\psi}{\partial r} = r\Omega_k^2\left(1+\frac{d\ln\Omega_k}{d\ln r}\frac{z^2}{r^2}\right), \tag{A6}$$

$$\frac{\partial\psi}{\partial z} = \Omega_k^2 z. \tag{A7}$$

We have used eq. (A7) to determine the vertical structure of the accretion flows [see eq. (16)].

We then integrate the basic equations in the vertical direction. The integrations of the continuity equation (eq. [5]) and the azimuthal component of the Euler equation (eq. [8]) are straightforward. In the process of the integration of the radial component of the Euler equation, we encounter the following integration:

$$\int_{-\infty}^{\infty}\rho\frac{\partial\psi}{\partial r}dz = \Sigma r\Omega_k^2 + W\frac{d\ln\Omega_k}{dr}. \tag{A8}$$

The last term in the right hand side of eq. (A8) is sometimes omitted in the height-integrated equations which appear in the papers on the accretion disks, which is not proper, since it can be the same order as the other terms in the Euler equation.

The left hand sides of the energy equations (eq. [11], eq. [12]) together with the thermodynamic relations (eq. [14], eq. [15]) are transformed to give

$$\rho T\left(v_r\frac{\partial s}{\partial r}+v_z\frac{\partial s}{\partial z}\right) = \frac{\gamma}{\gamma-1}\left[\frac{1}{r}\frac{\partial}{\partial r}\left(rv_rp\right)+\frac{\partial}{\partial z}\left(v_zp\right)\right]-v_r\frac{\partial p}{\partial r}-v_z\frac{\partial p}{\partial z}. \tag{A9}$$

We can integrate Equation (A9) with the integration

$$\int_{-\infty}^{\infty}v_z\frac{\partial p}{\partial z}dz = -Wv_r\frac{d\ln H}{dr}, \tag{A10}$$

to obtain the height-integrated version of the Energy equations (eq. [22], [23]).

B. Calculation of The Flux of Unscattered Photons

Consider the isothermal plane parallel atmosphere with the density distribution being

$$\rho(z) = \rho(0)\exp\left(-\frac{z^2}{2H^2}\right). \tag{B1}$$

Assuming the Eddington Approximation which is valid for isotropic radiation fields (and even for slightly nonisotropic fields, see Rybicki & Lightman 1979), the radiation field in the vertical direction is described by the radiative diffusion equation:

$$\frac{1}{3}\frac{\partial^2 J_\nu}{\partial \tau_\nu^2} = J_\nu - B_\nu, \tag{B2}$$

where τ_ν is the optical depth from the surface of the accretion flow. There is no well-defined surface of the accretion flow since the density tends to zero when we increase z but will never equals to zero [see eq. (B1)]. However, the optical depth τ_ν of the accretion flow in the vertical direction is finite and hence we can define the surface when the vertical height is measured with the optical depth. Note that $\tau = \tau_\nu^* = \frac{\sqrt{\pi}}{2}\kappa_\nu(0)H$ at the equatorial plane and $\tau = 2\tau_\nu^*$ at the other surface. We solve eq. (B2) with boundary conditions. We take

$$\begin{aligned} &\tfrac{1}{\sqrt{3}}\tfrac{\partial J_\nu}{\partial \tau_\nu} = J_\nu \quad (\tau_\nu = 0), \\ &\tfrac{\partial J_\nu}{\partial \tau_\nu} = 0 \quad (\tau_\nu = \tau_\nu^*). \end{aligned} \tag{B3}$$

The boundary condition at the surface assumes there is no irradiation onto the surface of the accretion flow and is derived by adopting two-stream approximation (see Rybicki & Lightman 1979). The solution for eq. (B2) which satisfies the boundary conditions [eq. (B3)] is

$$J_\nu = B_\nu\left\{1 - \frac{e^{-\sqrt{3}\tau_\nu}}{2}\left[e^{-2\sqrt{3}(\tau_\nu^* - \tau_\nu)} + 1\right]\right\}, \tag{B4}$$

The energy flux F_ν on the surface of the accretion flow is given by

$$F_\nu(0) = \frac{4\pi}{3}\left.\frac{\partial J_\nu}{\partial \tau_\nu}\right|_{\tau_\nu=0} = \frac{2\pi}{\sqrt{3}}B_\nu\left[1 - \exp\left(-2\sqrt{3}\tau_\nu^*\right)\right]. \tag{B5}$$

Note that

$$\begin{aligned} &F_\nu(0) = \tfrac{2\pi}{\sqrt{3}}B_\nu \quad (\tau_\nu^* \gg 1), \\ &F_\nu(0) = \tfrac{\sqrt{\pi}}{2}\chi_\nu(z=0)\,H \quad (\tau_\nu^* \ll 1). \end{aligned} \tag{B6}$$

REFERENCES

Abramowicz, M. A., Chen, X., Kato, S., Lasota, J.-P., & Regev, O. 1995, ApJ, 438, L37

Abramowicz, M. A., Czerny, B., Lasota, J. P., & Szuszkiewicz, E. 1988, ApJ, 332, 646

Bjornsson, G., Abramowicz, M. A., Chen, X., & Lasota, J. P. 1996, ApJ, 467, 99

Chen, X., Abramowicz, M. A., & Lasota, J. P. 1997, ApJ, 476, 61

Coppi, P. S. & Blandford, R. D. 1990, MNRAS, 245, 453

Dermer, C. D., Liang, E. P., & Canfield, E. 1991, ApJ, 369, 410

Duschl, W. J., Beckert, T., Mezger, P. G., & Robert, Z. 1996, in Physics of Accretion Disks, ed. Kato, S., Inagaki, S., Mineshige, S., Fukue, J. (Gordon and Breach Science Publishers), p. 91

Esin, A. A., Narayan, R., Ostriker, E., & Yi, I. 1996, ApJ465, 312

Genzel, R., & Townes, C. H. 1987, Ann. Rev. Astron. Astrophys., 25, 377

Honma., F. 1996, PASJ 48, 77

Ichimaru, S. 1977, ApJ, 214, 840

Jones, F. C.,1968, Phys. Rev., 167, 1159

Kato, S., Abramowicz, M. A., & Chen, X. 1996, PASJ, 48, 67

Kusunose, M., & Mineshige, S. 1996, ApJ, 468, 330

Manmoto, T., Takeuchi, M., Mineshige, S., Matsumoto, R., & Negoro, H. 1996, ApJ, 464, L135

Matsumoto, R., Fukue, J., Kato, S., & Okazaki, A. S. 1984, PASJ, 36, 71

Matsumoto, R., Kato, S., & Fukue, J. 1985, in Theoretical Aspects on Structure, Activity and Evolution of Galaxies III, ed. Aoki, S., Iye, M., & Yoshii, Y. (Tokyo Astronomical Observatory, Tokyo), p.102

Nakamura, E. K., Matsumoto, R., Kusunose, M., & Kato, S., 1996, PASJ 48, 761

Nakamura, E. K., Matsumoto, R., Kusunose, M., & Kato, S., 1997, PASJ submitted

Narayan, R. 1996, in Physics of Accretion Disks, ed. Kato, S., Inagaki, S., Mineshige, S., Fukue, J. (Gordon and Breach Science Publishers), p. 15

Narayan, R., Kato, S., & Honma, F. 1997, ApJ, in press

Narayan, R., & Yi, I. 1995, ApJ, 452, 710

Narayan, R., & YI, I., Mahadevan, R. 1995, Nature 374, 623

Paczyński, B., & Wiita, P.J. 1980, A&A88, 23

Piran, T. 1978, ApJ, 221, 652

Rybicki, G. B. & Lightman, A. P. 1979, Radiative Processes in Astrophysics (New York: John Wiley & Sons)

Shakura, N. I., & Sunyaev, R. A. 1973, A&A, 24, 337

Shapiro, S. L., Lightman, A. P., & Eardley, D. M. 1976, ApJ, 204, 187

Stepney, S., & Guilbert, P. W. 1983, MNRAS204, 1269

This manuscript was prepared with the AAS LaTeX macros v4.0.

Fig. 1.— The amount of the heating and the cooling rates for the ions (upper panel) and for the electrons (lower panel) in the units of $2\pi r^2/(\dot{M}W_i/\Sigma)$ and $2\pi r^2/(\dot{M}W_e/\Sigma)$, respectively. The ratio of advective cooling of ions to the viscous heating f is also shown in the upper panel. The accretion flow becomes advection dominated ($f = 1$) as the radius decreases and the energy transport from the ions to the electrons becomes practically zero. The radiative cooling is balanced with the electron advective *heating* in the innermost region.

Fig. 2.— The temperature of the ions and the electrons as a function of r. The electrons attain the temperature of 10^{10}K.

Fig. 3.— The aspect ratio h/r of the accretion flow.

Fig. 4.— The angular momentum (upper panel) and the various velocities (lower panel) of the accretion flow. The azimuthal velocity v_φ is highly sub-Keplerian. In the hot luminous region near the central black hole, the divergence of the velocities from those in the self-similar solution is fairly large.

Fig. 5.— The luminosity distribution as a function of r. The contributions from respective radiation mechanisms (i.e. bremsstrahlung, synchrotron, Comptonization) are also shown. The synchrotron emission and the Compton scattering dominate in the innermost region. The distribution of the bremsstrahlung emission is relatively flat.

Fig. 6.— The spectrum generated by the optically thin accretion flow around the central black hole of the mass $M_{\rm BH} = 10^8 M_\odot$. S indicates the synchrotron peak which comprises Rayleigh-Jeans slope and the optically thin synchrotron emission. C1 and C2 indicate the once and twice Compton scattered photons, respectively and B indicates the bremsstrahlung emission plus photons suffering multiple Compton scattering. W indicates saturated Comptonized photons.

Fig. 7.— The surface density (upper panel) and the temperature (lower panel) of the accretion flow. The dashed line corresponds to the case where $M_{\rm BH} = 10 M_\odot$. We find that the structure of the accretion flow is nearly the same when the radius and the mass accretion rate are scaled with the Schwarzschild radius and the critical mass accretion rate, respectively, while the electron temperature at the innermost region is varied slightly.

Fig. 8.— The spectrum generated by the optically thin accretion flow around the central black hole of the mass $M_{\rm BH} = 10 M_\odot$. The letters indicate the same meaning as Fig. 6. The shape of the spectrum is essentially the same. However, the position of the synchrotron peak and the total luminosity differ significantly.

Fig. 9.— The spectrum of Sgr A* (upper panel). The lines correspond to the spectrum calculated with our model presented in this paper. The $\dot{M}$-dependence of the spectrum and the temperature and the surface density (lower panel) are illustrated. The spectra behaves in the simplest way. When $\dot{M}$ is reduced, the surface density and the entire emission are also reduced. The bremsstrahlung emission is more sensitive to the $\dot{M}$ change than the synchrotron emission.

Fig. 10.— The $M_{\rm BH}$-dependence of the spectrum (upper panel) the temperature and the surface density (lower panel). The position of the Rayleigh-Jeans slope determines the mass of the central black hole. The surface density is not varied when $M_{\rm BH}$ is changed.

Fig. 11.— The β-dependence of the spectrum (upper panel) the temperature and the surface density (lower panel). When β is lowered, the temperature decreases and the bremsstrahlung emission is weakened. However, the synchrotron emission is fairly insensitive to the change of β.

Fig. 12.— The α-dependence of the spectrum (upper panel) the temperature and the surface density (lower panel). When α is lowered, the surface density increases and so the

bremsstrahlung emission. However, the synchrotron emission weakened due to the decrease of the electron temperature in the innermost region.

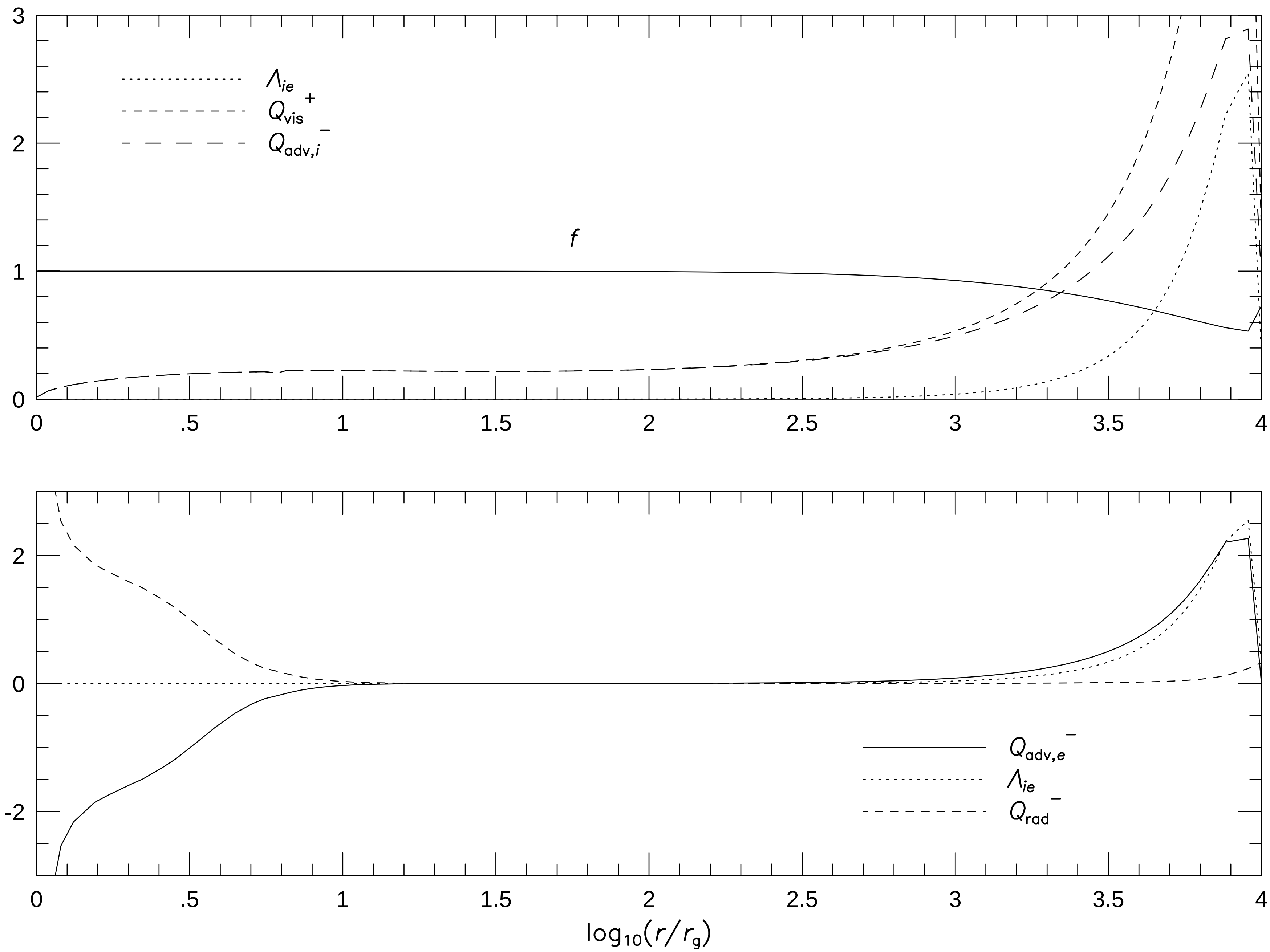

Λ_{ie} +
$Q_{\rm vis}$
$Q_{{\rm adv},i}$ −
f
$Q_{{\rm adv},e}$ −
Λ_{ie}
$Q_{\rm rad}$ −
$\log_{10}(r/r_{\rm g})$

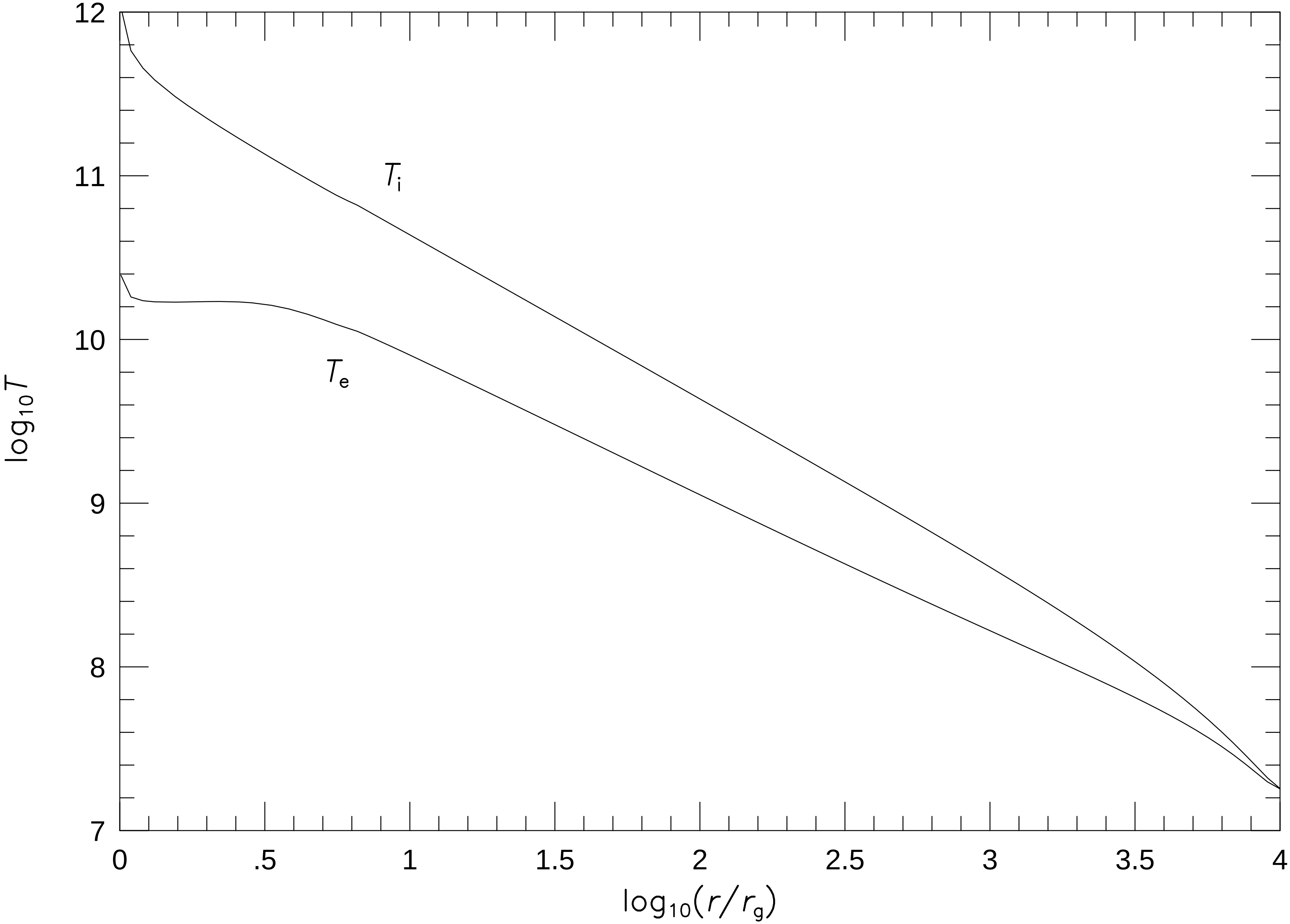

12
11
10
9
8
7
0
.5
1
1.5
2
2.5
3
3.5
4
$\log_{10} T$
$\log_{10}(r/r_g)$
T_i
T_e

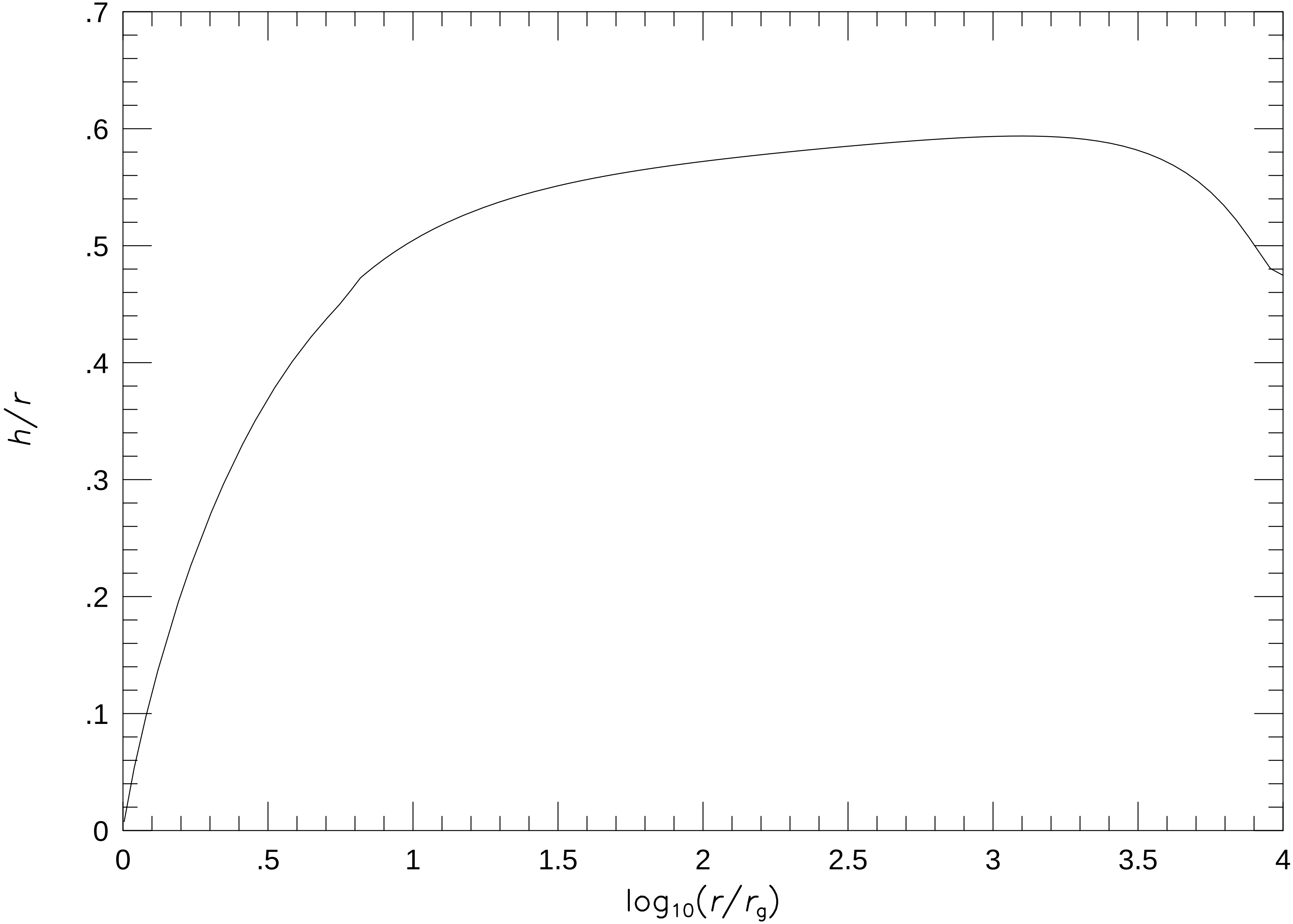

.7
.6
.5
.4
.3
.2
.1
0
0
.5
1
1.5
2
2.5
3
3.5
4
h/r
$\log_{10}(r/r_g)$

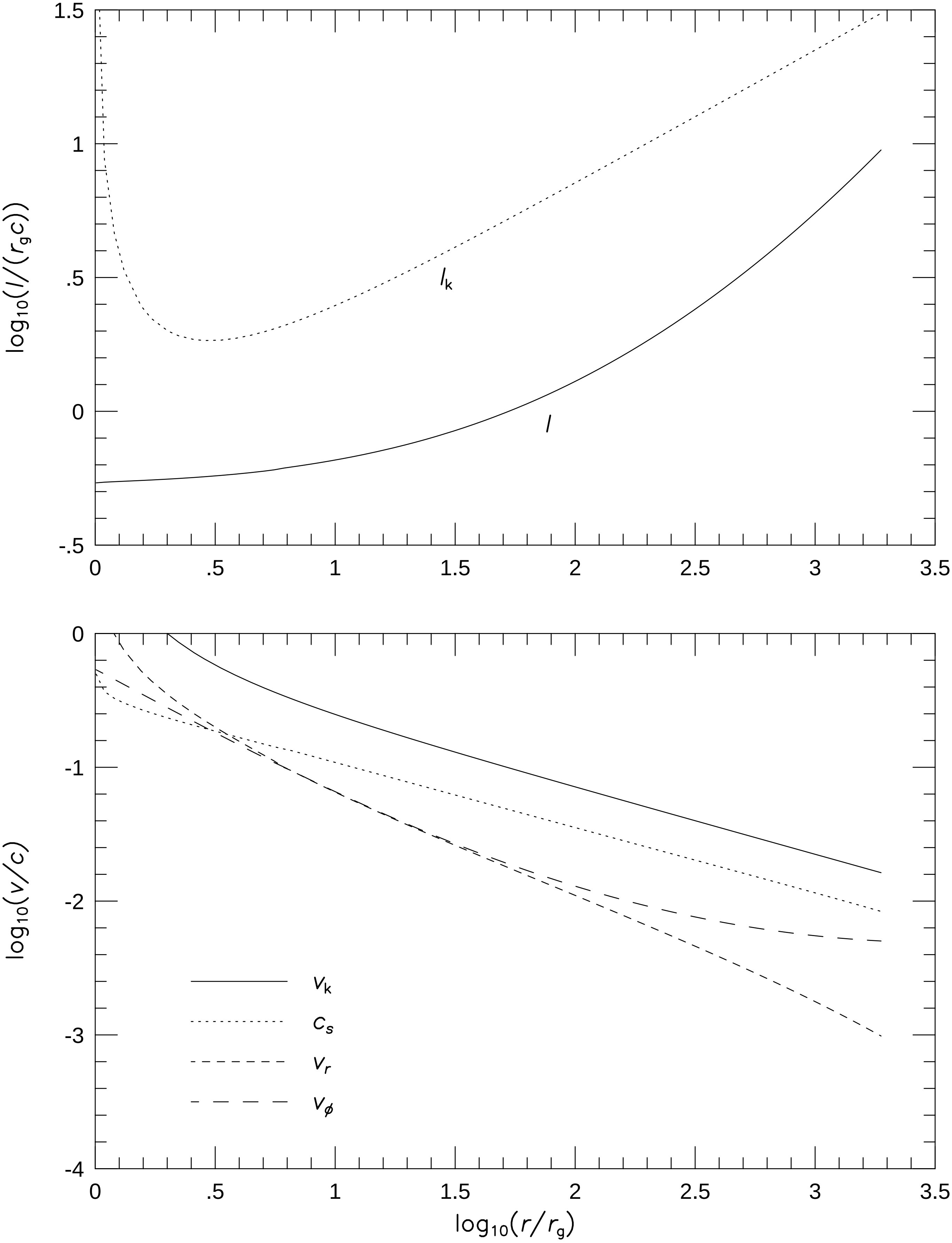

$\log_{10}(l/(r_g c))$
l_k
l
$\log_{10}(v/c)$
v_k
c_s
v_r
v_ϕ
$\log_{10}(r/r_g)$

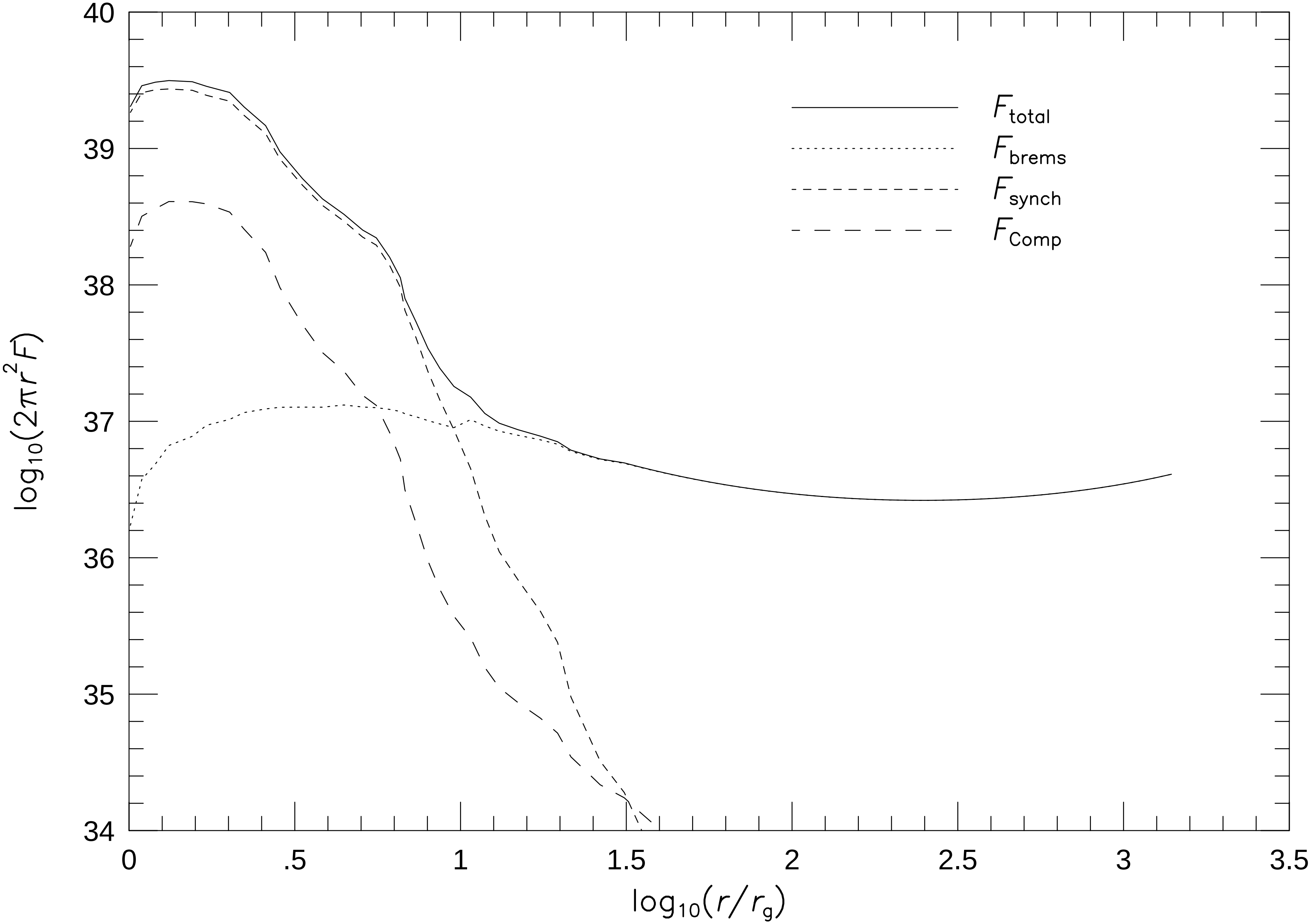

F_{total}
F_{brems}
F_{synch}
F_{Comp}
$\log_{10}(2\pi r^2 F)$
$\log_{10}(r/r_g)$
40
39
38
37
36
35
34
0
.5
1
1.5
2
2.5
3
3.5

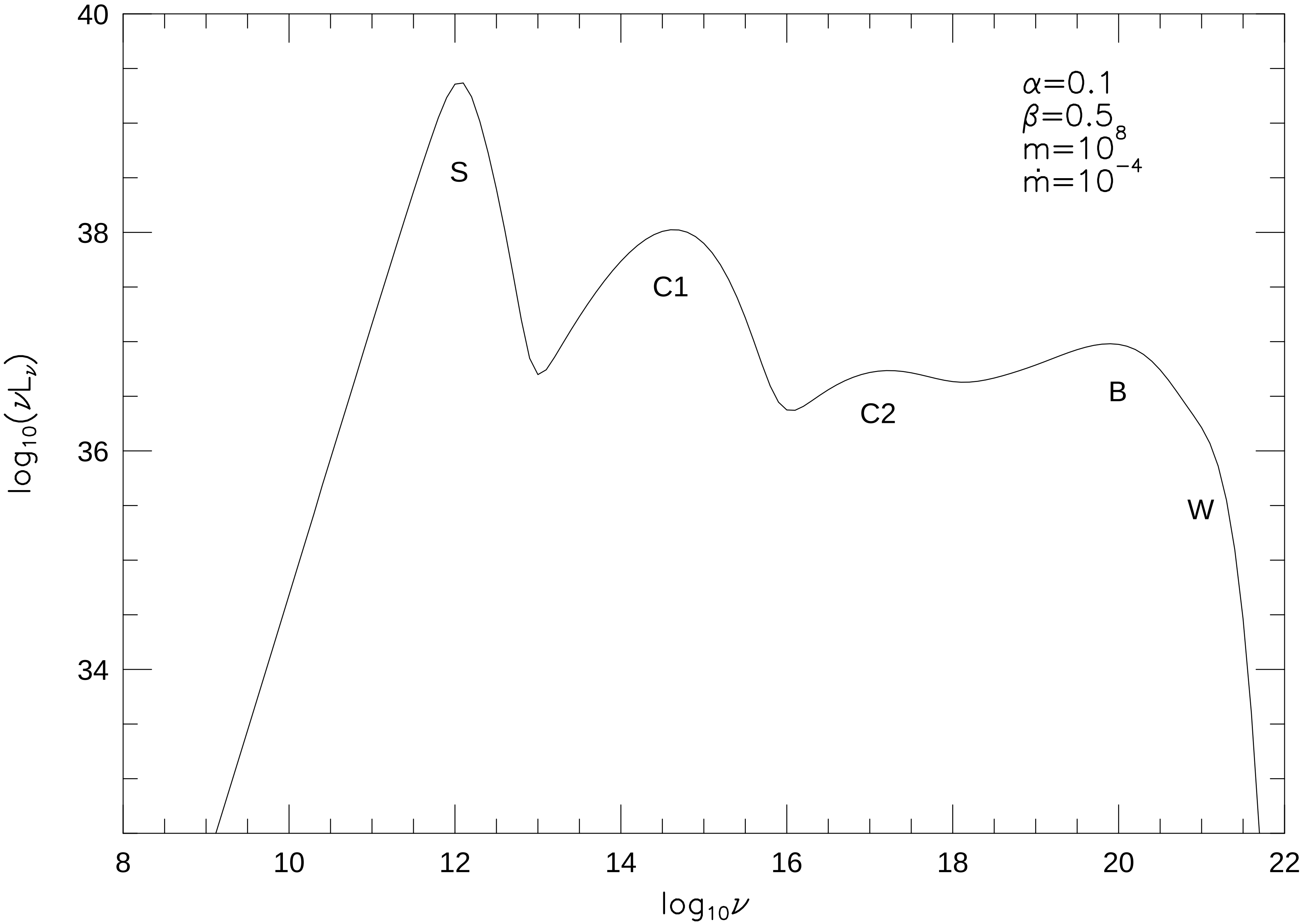

α=0.1
β=0.5
m=10^8
ṁ=10^-4
S
C1
C2
B
W
40
38
36
34
8
10
12
14
16
18
20
22
log10(νLν)
log10ν

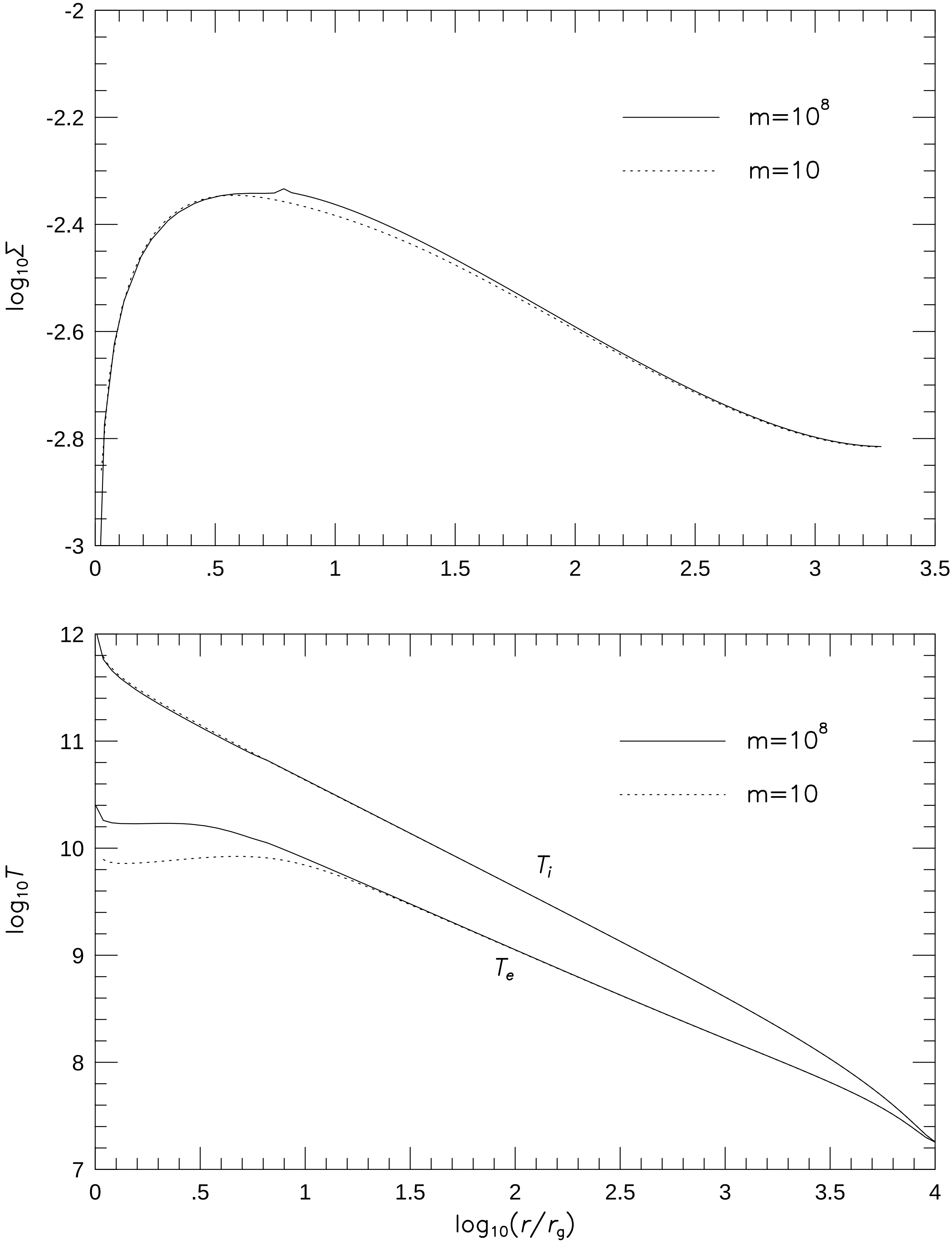

m=10^8
m=10
log10Σ
-2
-2.2
-2.4
-2.6
-2.8
-3
0
.5
1
1.5
2
2.5
3
3.5
m=10^8
m=10
T_i
T_e
log10T
12
11
10
9
8
7
0
.5
1
1.5
2
2.5
3
3.5
4
log10(r/r_g)

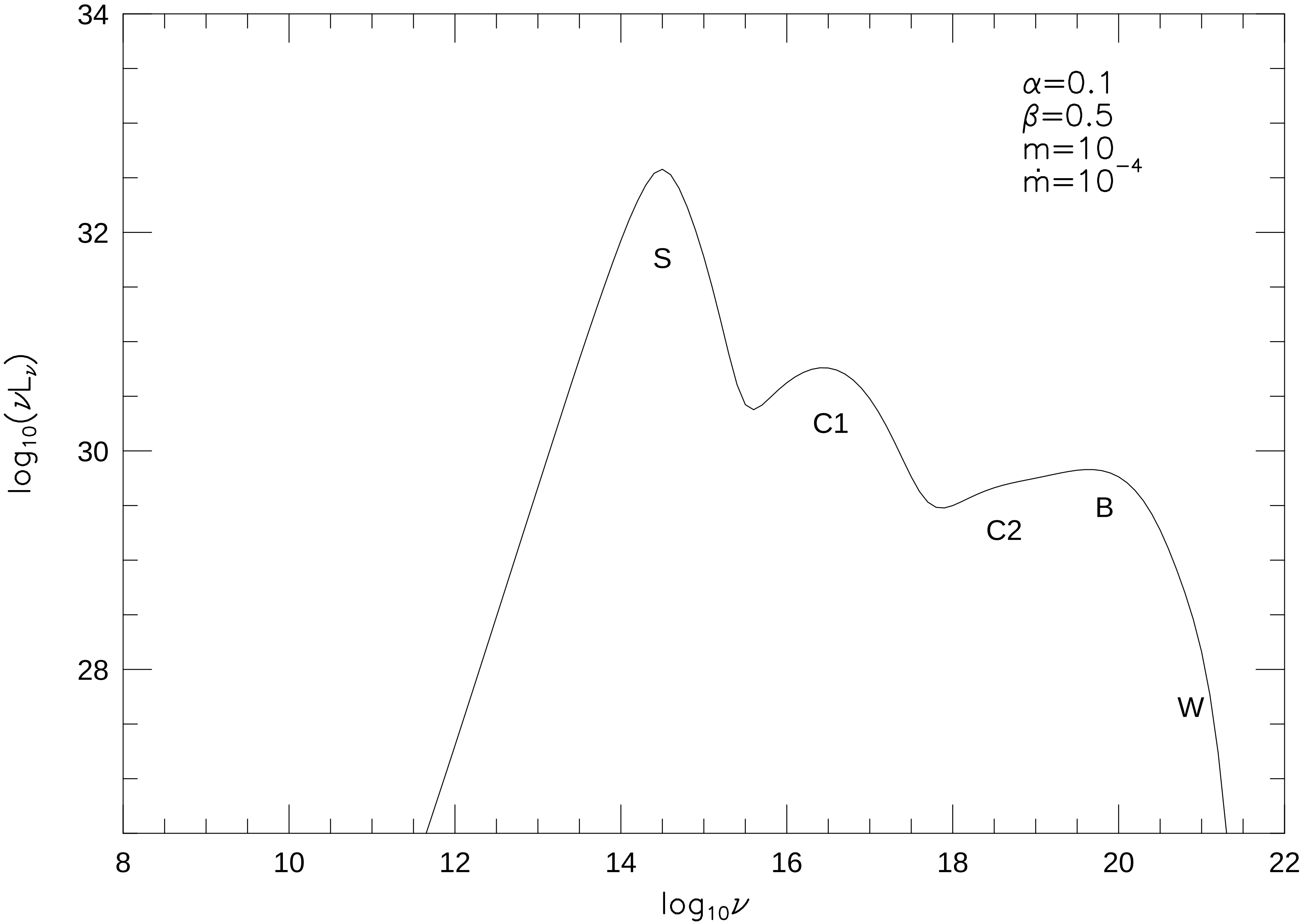

α=0.1
β=0.5
m=10
$\dot{m}$=10^{-4}
S
C1
C2
B
W
34
32
30
28
8
10
12
14
16
18
20
22
$\log_{10}\nu$
$\log_{10}(\nu L_\nu)$

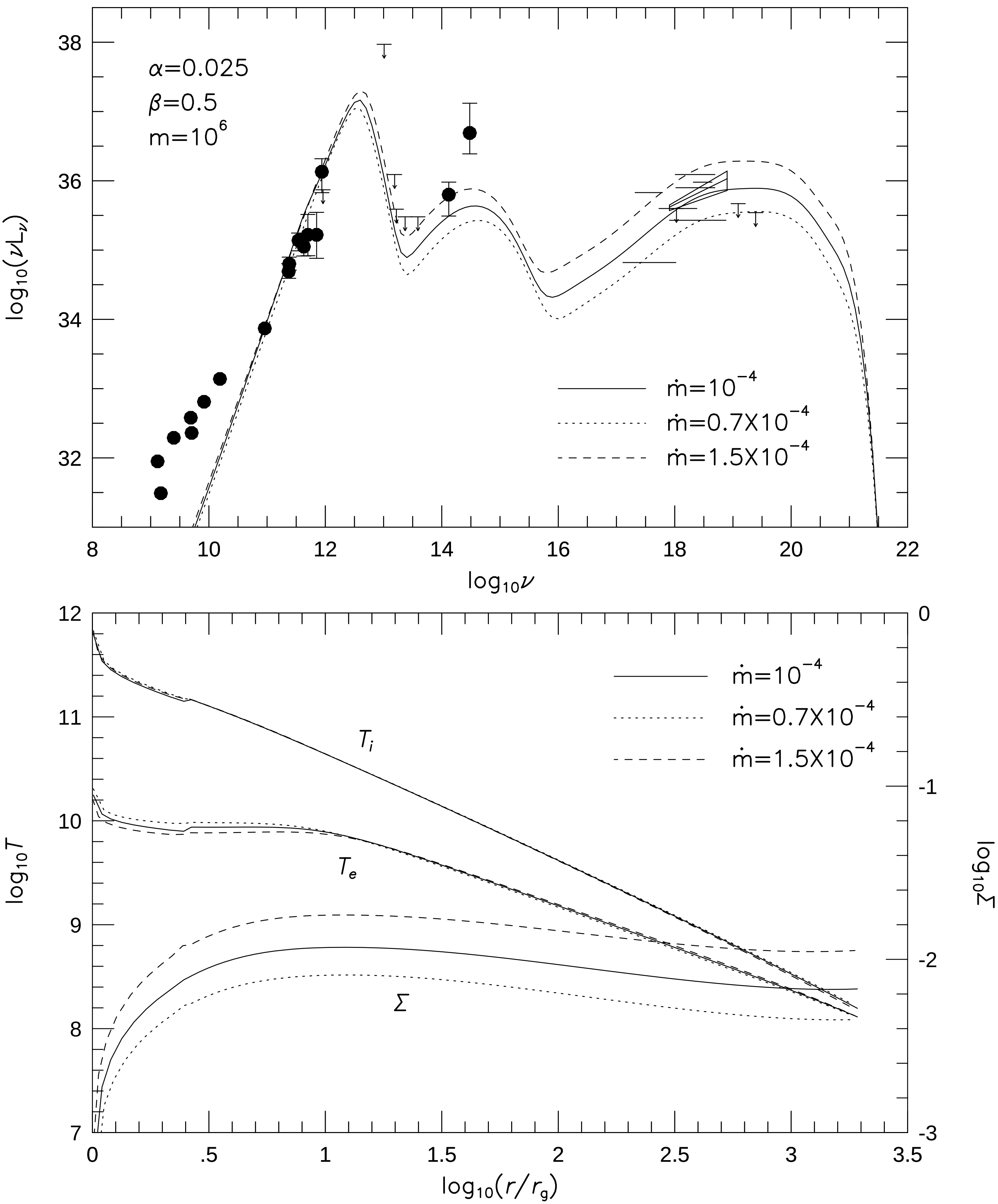

α=0.025
β=0.5
m=10^6
ṁ=10^-4
ṁ=0.7X10^-4
ṁ=1.5X10^-4
log10(νLν)
log10ν
38
36
34
32
8
10
12
14
16
18
20
22
log10T
log10Σ
log10(r/rg)
Ti
Te
Σ
12
11
10
9
8
7
0
-1
-2
-3
0
.5
1
1.5
2
2.5
3
3.5

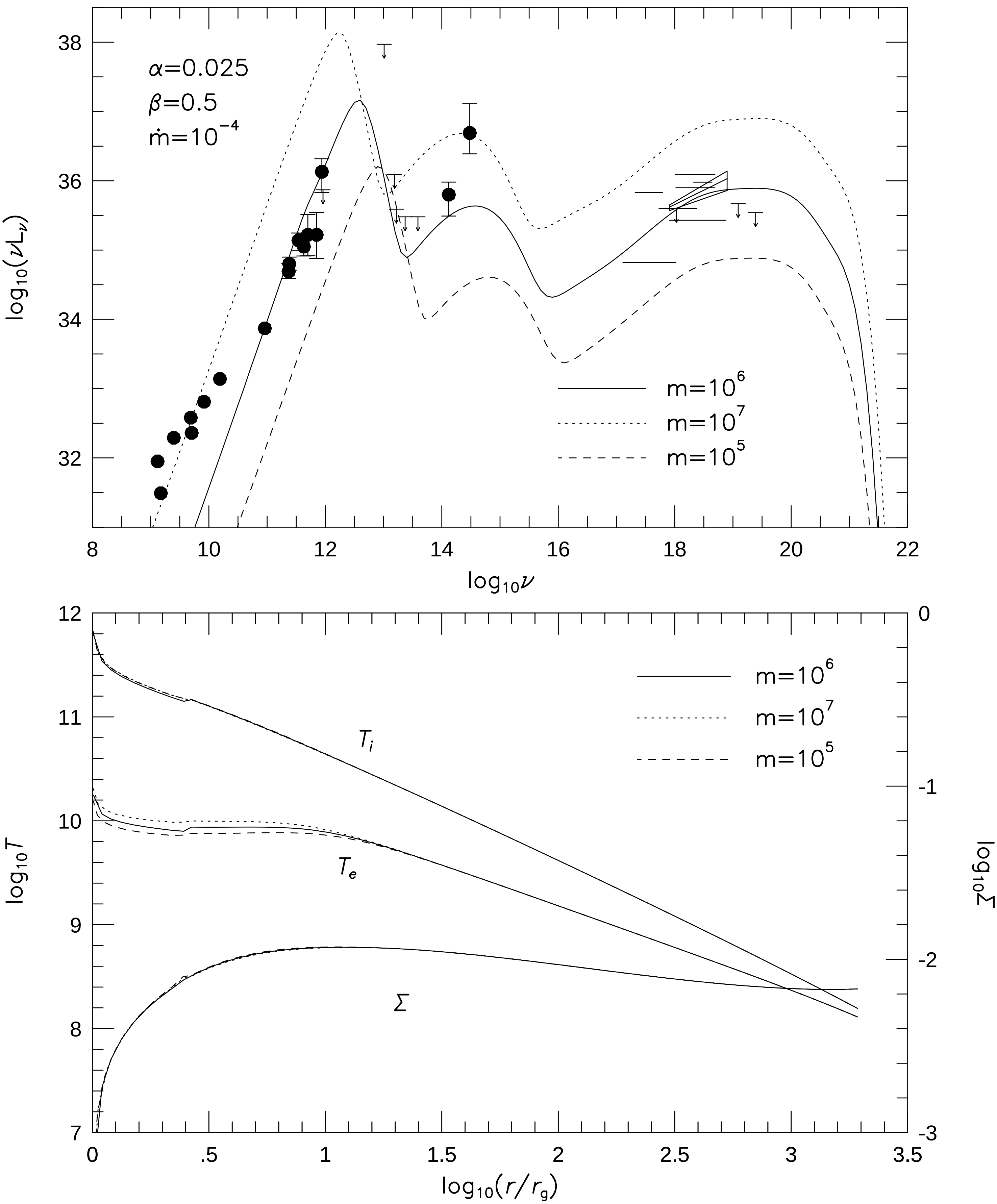

α=0.025
β=0.5
ṁ=10^-4
m=10^6
m=10^7
m=10^5
log10(νLν)
log10ν
T_i
T_e
Σ
log10T
log10Σ
log10(r/rg)

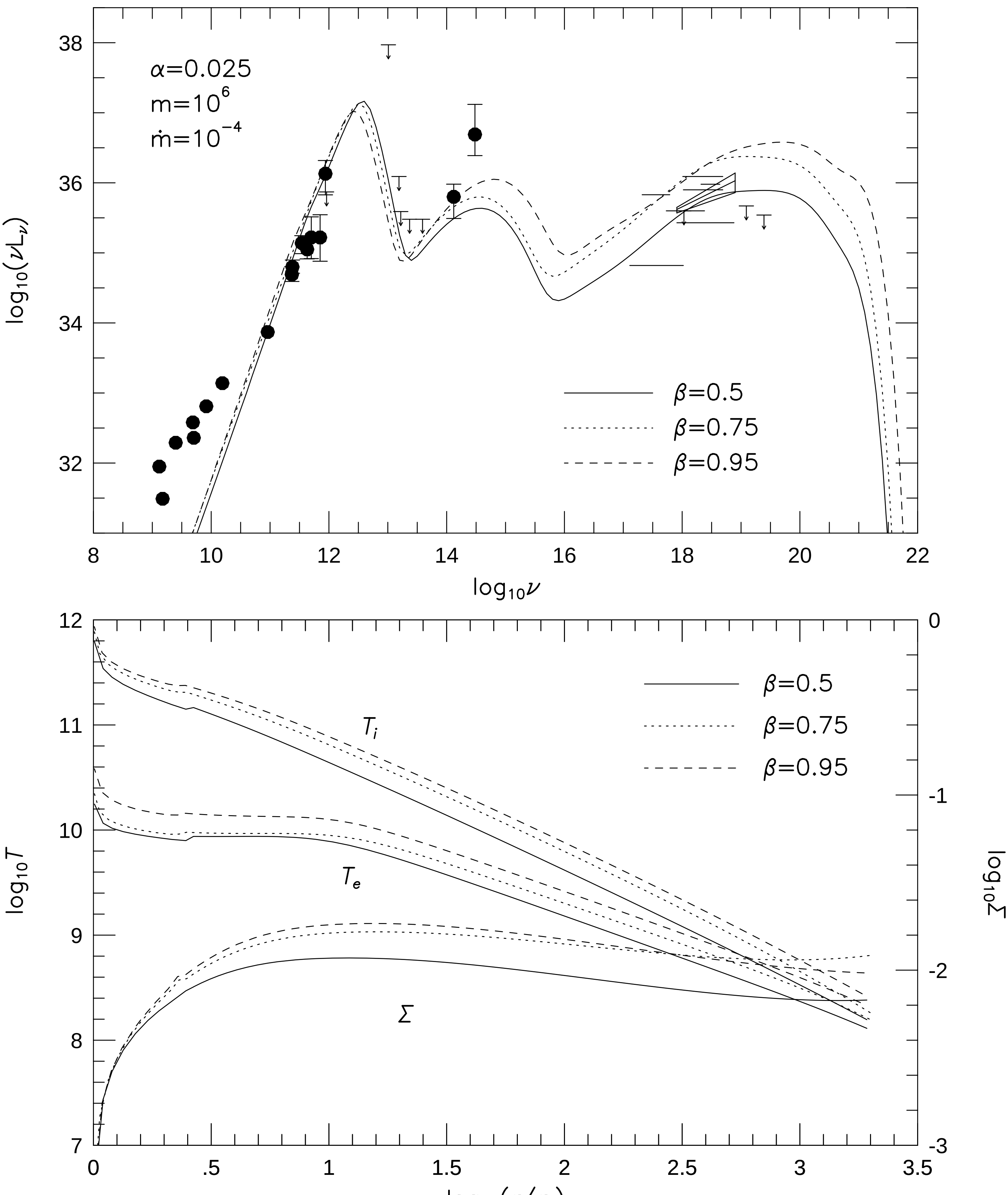

α=0.025
m=10^6
ṁ=10^-4
β=0.5
β=0.75
β=0.95
log10(νLν)
log10ν
T_i
T_e
Σ
log10T
log10Σ
log10(r/rg)

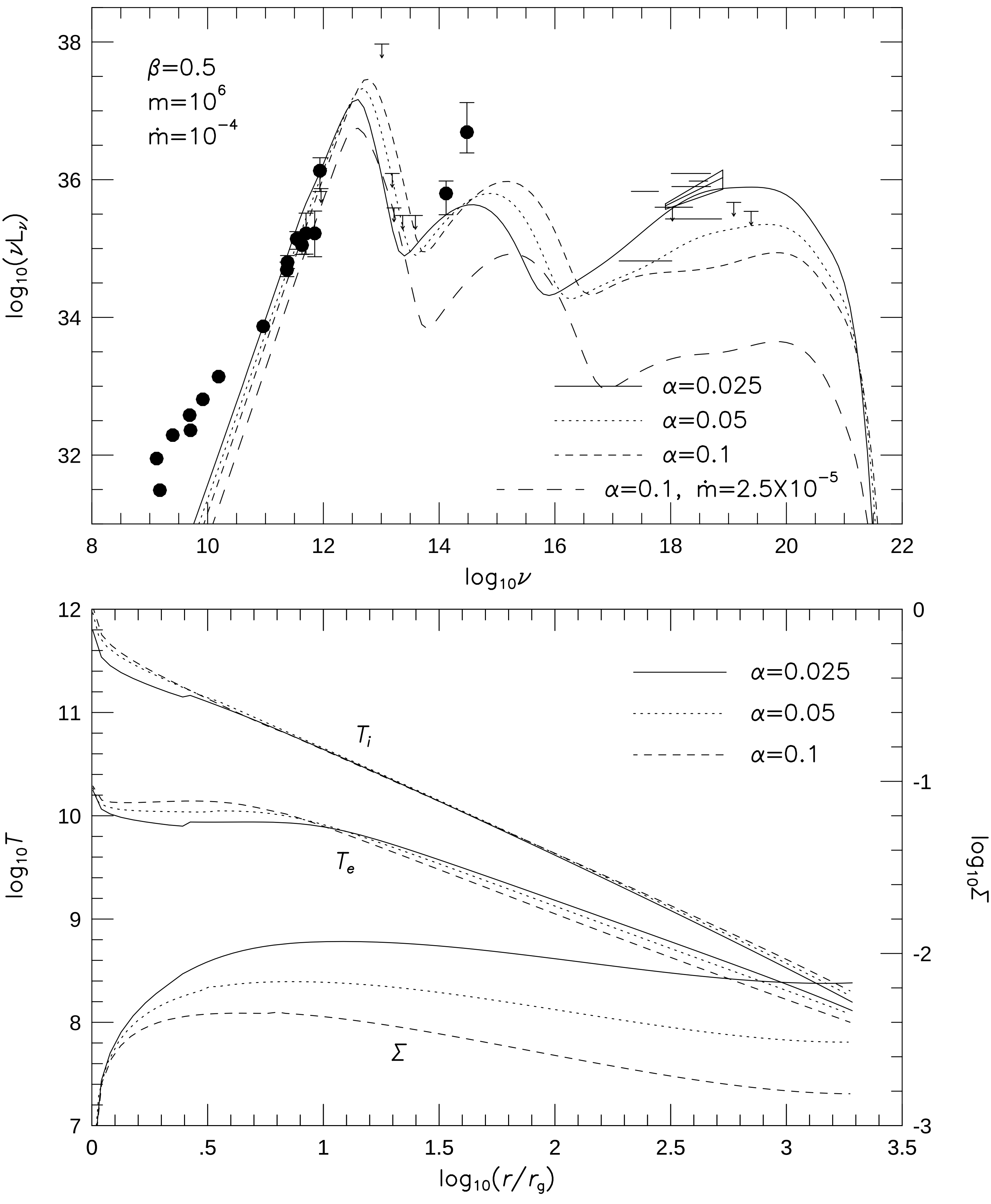

β=0.5
m=10^6
ṁ=10^-4
α=0.025
α=0.05
α=0.1
α=0.1, ṁ=2.5X10^-5
log10(νLν)
log10ν
T_i
T_e
Σ
log10T
log10Σ
log10(r/r_g)